Received: 27 September 2024 | Revised: 2 December 2024 | Accepted: 27 December 2024 | Published online: 21 January 2025

RESEARCH ARTICLE

Journal of Optics and Photonics Research
2026, Vol. 3(2) 174–186
DOI: 10.47852/bonviewJOPR52024397

BON VIEW PUBLISHING

Reliability Analysis of Residential Buildings Under Hurricane Using Embedded FBG Sensors: Remaining Useful Lifetime Analysis

Abolghassem Zabihollah[1,*] and Yu Shi[2]

[1]*Department of Mechanical, Environmental, and Civil Engineering, Tarleton State University, USA*

[2]*Department of Mathematics, Tarleton State University, USA*

Abstract: Every year, the lack of reliable and affordable structural health monitoring systems to assess the resilience of residential buildings in coastal areas results in extensive damage from strong winds and hurricanes. This work investigates the use of embedded fiber Bragg grating (FBG) sensors for the structural health monitoring of residential timber buildings for reliability assessment. The remaining useful lifetime (RUL) of buildings after being impacted by hurricane has been estimated using long short-term memory (LSTM) neural network. A proof-of-concept experimental setup has validated the system's performance and functionality. Multiple one-story and two-story scaled-down (∼1:20) prototype timber buildings were constructed and placed in a wind tunnel to assess their structural performance and stability under wind speeds ranging from 0 to 150 mph. FBG sensors attached to the buildings measured strain in real time. The measured strain data are used to estimate the building's reliability. A mathematical Health Indicator is introduced to determine the level of structural integrity and health under varying load and structural conditions. The FBG sensors demonstrated accurate measurement and real-time monitoring of strain changes in selected structural elements during high wind speeds. Assessment results can inform condition-based maintenance, safety evaluations, and stability reports. Additionally, the system can issue real-time warnings for potential failures and damages, thereby enhancing the overall resilience of residential buildings.

Keywords: residential building, hurricane, FBG, stability, remaining useful lifetime, long short-term memory

1. Introduction

Annually, strong winds, hurricanes, and tornadoes inflict significant damage and claim lives in coastal regions, prompting researchers in the structural health monitoring (SHM) community to develop cost-effective monitoring systems for residential buildings. While civil infrastructure like bridges and tunnels, as well as critical buildings such as hospitals and high-rises, have benefited from SHM systems for a decade, these systems remain prohibitively expensive for residential use. An SHM system typically includes an array of sensors, a signal processing unit, and a communication platform for timely reporting and issuing evacuation or maintenance recommendations. Reports generated by the monitoring system are utilized by local authorities, construction firms, insurance providers, and real estate agents to assess the structure's safety and reliability, enabling appropriate actions to safeguard residents' lives.

There are multiple hazards associated with hurricanes, including high winds, storm surges, and waves, as well as wind-driven rain, wind-borne debris, and flood-borne debris, along with scour and erosion. As a result of these hazards, buildings may fail in several ways, including building envelope failure caused by high winds and debris impact, and consequent water infiltration due to heavy rainfall and wind-driven rain. Perhaps the occurrence of hurricanes is the most common weather condition issues leading to catastrophic damages in residential buildings particularly in coastal areas [1]. A hurricane arises from atmospheric turbulence, generating high winds (90–135 mph) that exert strong forces on structures. Traditionally, mitigating hurricane damage involves hardening homes [2]. However, devising effective hardening or mitigation strategies requires assessing structural performance and health conditions. Accurate estimation of potential losses is crucial for implementing condition-based mitigation efforts to reduce future losses. Numerous studies have been conducted to estimate hurricane damage across various types of structures [3]. A critical aspect in predicting damage from future hurricanes is the development and accumulation of micro-damage resulting from multiple hurricane events.

This phenomenon can gradually weaken the structure, potentially leading to sudden failure even under forces lower than intended. Current evaluation methods for residential buildings primarily rely on visual inspection due to their affordability and simplicity. However, the accuracy of visual inspection is heavily reliant on the inspector's experience, making it susceptible to human errors. Moreover, visual inspections are conducted periodically and do not offer continuous information about the

***Corresponding author:** Abolghassem Zabihollah, Department of Mechanical, Environmental, and Civil Engineering, Tarleton State University, USA. Email: azabihollah@tarleton.edu

building's condition between inspections. The SHM system comprises sensors, data acquisition and transmission systems, and a database for efficient data management and health diagnosis, including damage detection, safety evaluation, and reliability analysis. Over the past two decades, significant research has focused on enhancing the accuracy and functionality of each component of SHM systems [4]. SHM technology plays a crucial role in evaluating the safety and durability of structures during and after hurricanes, ensuring their continued serviceability and sustainability [5]. By offering precise and real-time damage assessment, SHM helps prevent catastrophic damage, provides early disaster warnings, and ultimately saves lives during environmental disasters like hurricanes. SHM systems applied to civil infrastructures such as bridges and high-rise buildings involve monitoring the structure by assessing its performance during operation.

Sivasuriyan et al. [6] investigated the use of accelerometers for operational monitoring and damage evaluation of multi-story buildings. Most of the existing SHM systems use electrical sensors, including strain gauges, piezoelectric, and linear variable differential transformers. Piezoelectric sensors are relatively low-cost sensors that provide sufficient accuracy to be used in residential buildings. Maraveas and Bartzanas [7] conducted a review on the application of various sensor types and technologies for SHM of agricultural structures. Park and Inman [8] explored the use of piezoelectric sensors for detecting damage in buildings through impedance measurements. The effectiveness of piezoelectric sensors in SHM depends significantly on their placement within the structure, necessitating optimization algorithms to determine sensor count and optimal locations [9].

More recently, fiber Bragg grating (FBG) sensors have gained prominence in SHM systems for civil infrastructure, including dams and high-rise buildings [10]. Braunfelds et al. [10] investigated the application of FBG sensors for monitoring the structural integrity of road asphalt. Sliti and Boudriga [11] utilized FBG sensors for vibration monitoring of buildings, particularly for assessing structural performance during earthquakes.

Amaya and Sierra-Pérez [12] employed embedded FBG sensors to monitor the structural health of reinforced concrete structures. They utilized wavelength changes as indicators to monitor structural integrity variations caused by different excitation frequencies. Wu et al. [13] summarized the contemporary applications of fiber optic sensors for SHM in buildings. The applicability of residential buildings under hurricanes using FBG sensors has been explored by Zabihollah et al. [14].

Despite valuable research work in usefulness of FBG sensors for real-time structural heal monitoring of buildings, there is a lack of knowledge in accurate modeling for estimating the remaining life of the buildings which have experienced hurricane attacks.

The studying of reliability analysis of FBG sensor has been a challenging task in the field of civil infrastructure. Liu et al. [15] used failure model and effects analysis techniques to access ascertain critical failure items including failure modes, failure causes, and effects. It returns a risk priority number to map to which risk item is, and then it can apply in various engineering applications such as full-scale structural testing of wind turbine blades.

Long short-term memory (LSTM) is a type of recurrent neural network (RNN) that was first introduced by Hochreiter and Schmidhuber in 1997 [16]. The principle of recurrent network is using feedback connections to store and represent their recent information from input. The original simple RNN is a series of blocks/units' structure that the information of each block depends on previous blocks and inputs, and it was first developed by Elman in 1990 [17] which operates with a structure of sequential blocks or units, where each block's information depends on previous blocks and inputs. This RNN sequential block design enables the modeling of time series problems and the prediction of future values based on past data. Consequently, this type of time series prediction model is also called a sequence-to-sequence model at each time point t, and there is an individual block that includes an input unit vector X_t, a hidden unit vector H_t, and an output unit vector Y_t.

Building on RNN foundation, Hou et al. [18] discussed the integrations of LSTM networks in building SHM. LSTM time series analysis predicts potential structural issues, enabling early warnings and informed maintenance decisions for civil infrastructures. LSTM networks have also been applied in safety monitoring under earthquake conditions, such as in the study of Zhang et al. [19], which developed a LSTM model to access building's reliability during seismic events. The LSTM model was also used by Miao et al. [20] to investigate the SHM of bridges under external loadings. It is trained by time series data from many factors in bridge and then predicts deterioration conditions.

The main contribution of this paper is the development of a data-driven LSTM model specifically tailored to estimate the remaining useful life (RUL) of FBG sensors embedded in buildings. This approach focuses on leveraging the time series strain data captured by FBG sensors to train an LSTM sequence-to-sequence model that estimates RUL, with a particular emphasis on the structural integrity of residential timber buildings subjected to wind loads and hurricane conditions. It also explores the feasibility of using FBG sensors to monitor strain and assess the structural integrity of residential timber buildings under wind loads and hurricane conditions. By utilizing strain data from embedded FBG sensors, the proposed LSTM model advances predictive maintenance strategies, estimating the RUL of structures impacted by hurricanes or strong winds and enabling timely intervention for risk mitigation.

2. Modeling Building with Embedded FBG Sensors

2.1. Dynamic modeling of timber building

A typical building structure can be approximated by frame structure (Figure 1(a)). For structural building, a 3-dimensional frame element (Figure 1(b)) has 5 degrees of freedom (displacement in x, y, z directions, and rotation about y and z axes) at each node in the local coordinate system.

Figure 1
Finite element modeling of a building: (a) 3D frame, (b) simplified 2D frame element

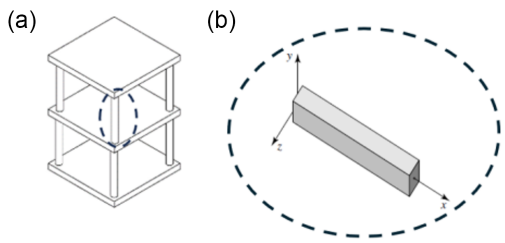

The dynamic response of a frame is given as:

$$[M]\{\ddot{d}\} + [D]\{\dot{d}\} + [K]\{d\} = \{F(t)\} \tag{1}$$

The terms M, D, and K are the mass, structural damping, and stiffness matrices, respectively. For the sake of brevity, the details of element matrices are skipped, however. For details of the finite element procedure, one may consult the book written by Reddy [21]. The displacement $\{d\}$ is a vector containing the nodal degrees of freedom (DOFs) (u, v, w, θ_y, and θ_z) of the element. The structural stability of the building can be estimated by accurate calculation of the induced stress at the critical elements in real time. For a frame structural element, the dominated stress is along the length of the element is:

$$\sigma_x = E\varepsilon_x \tag{2}$$

Equation (2) shows that stress is proportional to strain; therefore, accurate measurement of strain results in accurate determination of stress at elements. Furthermore, the element deflection is determined by accurate measurement of strain as given in Equation (3):

$$\varepsilon_x = -y\frac{d^2v}{dx^2} \tag{3}$$

For stability analysis of the structure subjected to hurricane's load, the force vector $\{f(t)\}$ in Equation (1) is determined as:

$$F(t)_{wind} = P_{wind}A \tag{4}$$

where A indicates the area of the element facing the wind and pressure due to wind, P_{wind}, is determined as:

$$P_{wind} = C_p\left(\frac{1}{2}\rho_{air}V_{wind}^2\right) \tag{5}$$

where ρ_{air}, C_p, and V_{wind} are density of air, shape coefficient of the building face the wind, and wind speed.

2.2. Strain measurement using FBG sensors

According to discussion provided in Section 2.1, the stability of the structure can be estimated by acquiring an accurate measurement of the strain induced in the element due to applied load. In the present research, embedded FBG sensors have been used to measure the strain within the elements. FBG sensors provide advantages such as multi and continuous sensing using only a single fiber line, ease of placing and embedding in the structure, and high sensitivity.

The principle of a FBG sensor is based on the wavelength shifting of the reflected spectrum when strain or temperature change arises in the element. The maximum reflectivity of FBG occurs at the Bragg wavelength, λ, given by:

$$\lambda_{FBG} = 2n_{eff}\tau_{FBG} \tag{6}$$

where n_{eff} is the effective refractive index of the mode propagating in the fiber and τ_{FBG} indicates the FBG period. Equation (6) implies that the reflected wavelength λ is affected by any variation in the physical or mechanical properties of the grating region. Similarly, changes in temperature lead to change in n_{eff} via the thermo-optic effect and in an unconstrained fiber; τ_{FBG} is influenced by thermal expansion or contraction. Considering the effect of variation of mechanical properties as k_T and that of the temperature as k_ϵ, Equation (6) can be written as:

$$\frac{\Delta\lambda_{FBG}}{\lambda_{FBG}} = k_T\Delta T + k_\varepsilon\Delta\varepsilon \tag{7}$$

Considering a constant temperature of the structure during testing, the induced strain on the element can be estimated as:

$$\Delta\varepsilon = \frac{\Delta\lambda_{FBG}}{k_\varepsilon} \tag{8}$$

For more details on modeling FBG for strain measurement, one may consult the work of Sarkandi and Zabihollah [22].

In the present work, a bare fiber optic cable (FBG-MR0010, purchased from Micronor Sensors, Inc.) composed of four FBG sensors with wavelength of 850 nm and 300 nm grating period that relocated 10 mm apart is used to determine the induced strain on the selected element of the frame. The FBG sensors provide strain and temperature measurement with a sensitivity of 1 μm/m and 0.1 °C, respectively. The fiber optic cable is connected to an FBGX100 Interrogator with a wavelength range of 808–880 nm (FISENS®). FBG sensors are affixed to the outer surface of the column (facing the wind force) using adhesive tape.

3. LSTM Neural Network Prediction of RUL Analysis

The main reason of degradation and reliability decrease is due to the strain happens on the surface and inside of building structures. Therefore, the cumulative strain and health index should be identified and mapped to reliability or RUL. In this research, the strain measure is collected by FBG sensor, and the detail will be discussed in Section 4.3. The FBG sensors continuously collect strain on building structure surface with unit of μm/m that is the increasing of strain is measured as some μm per meter in this research, and we use ε_t to represent the measure of strain on structure at time t. However, from the probability distribution theory, due to the random fluctuations across the structure, deriving a closed-form mathematical expression for the distribution of ε_t is challenging. In this context, big data and deep learning techniques are well-suited for predicting the RUL. From the background introduction in Section 1, it is clear that LSTM is a neural network model that is particularly suited for estimating the RUL of structures due to their ability to capture long-term dependencies in sequential data. Although other models, such as feedforward neural networks or simple RNNs, could also be applied, they lack the memory retention capability of LSTM networks, making them less suitable for capturing the time-dependent degradation patterns commonly observed in SHM.

3.1. Fundamental concept of RUL

Since the RUL represents the remaining time that the structure can be operable before its total failure, the mathematical formula of RUL at current time point t can be defined as:

$$RUL(t) = fail\_time - curr\_time \tag{9}$$

From structure theory and Hooke's law, the failure time can be defined as the point at which the surface experiences the

maximum strain that can be read from sensor directly, after which it begins to lose integrity. Thus, the failure time corresponds to the moment when maximum strain is reached:

$$fail\_time = time\_index(\max\ strain) \tag{10}$$

Since the current time t can be read from sensor directly, the RUL at time t can be obtained from Equation (9).

On the other hand, the measure of strain, ε_t, at any time point t can also be read from sensor. Thus, the cumulative strain can also be derived as:

$$Cumu(\varepsilon_t) = \sum_{j=0}^{t} \varepsilon_j \tag{11}$$

Therefore, the machine learning prediction model between cumulative strain $Cumu(\varepsilon_t)$ and $RUL(t)$ can be designed.

In this research, the training and testing datasets are all obtained from FBG sensor real-time collection. In both training and testing datasets, the only feature variable X is cumulative strain $Cumu(\varepsilon_t)$ while the target variable Y is $RUL(t)$. The data are collected under constant wind speed and dynamic wind speed cases. The constant wind speed dataset includes 11083 records while dynamic wind speed dataset includes 5244 records.

3.2. LSTM networks structures

Since the cumulative degradation increases with time, the LSTM RNN model should be developed to predict the RUL of the building structures.

In simple RNN framework as shown in Figure 2, at current time t, the current input information is represented by input unit X_t. Similar to logistic regression structure, X_t will be multiplied by a weight matrix W_{ht}; and XW passes through a non-linear activation function to compute the values of the hidden units H_t. Then, this hidden unit will be then used to calculate with another weight matrix Wot to get the corresponding output Y_t. So, the output in RNN network is following:

$$Y_t = \sigma(W_{ot}H_t + b_Y) \tag{12}$$

Figure 2
A simple RNN network

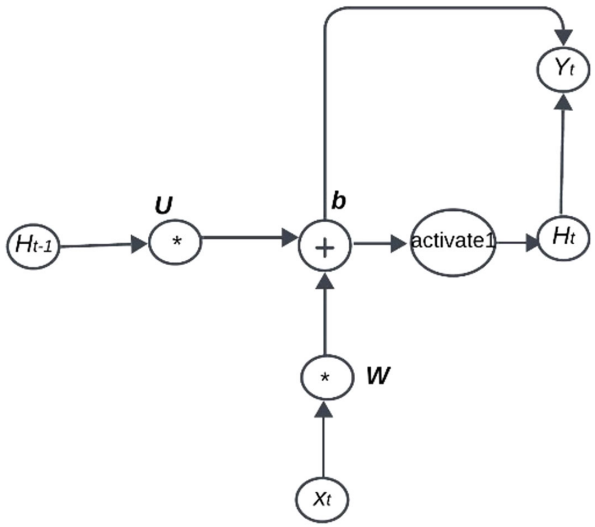

and

$$H_t = \delta(W_{ht}X_t + U_tH_{t-1} + b_H) \tag{13}$$

While U_t is the weight matrix that connect to the hidden unit H_{t-1} from previous block at time t-1. Therefore, the functional relationship between X_t and Y_t will be following:

$$Y_t = \sigma(W_{ot}\ \delta(W_{ht}X_t + U_tH_{t-1} + b_H) + b_Y\ ) \tag{14}$$

Both σ, δ are activation function in LSTM network, and the commonly used activation functions include sigmoid function, linear function, rectified linear unit function, and hyperbolic tangent function.

As it is observed, the RNN uses weight and bias matrix to update the information changing at each step and then use chain rule to go through until it arrives at the last time point. One of disadvantages of RNN is the vanishing gradient issue that makes the multiple layers of RNN models not easy to train and fit well. Hochreiter and Schmidhuber [16] mentioned that short-term and long-term dependencies information can be employed to build sequence models instead of traditional gradient methods. This idea is originally from natural language processing problems, and then it also applied to numerical regression or classification problems. LSTM algorithm is applied in engineering areas to monitor engineering reliability and health in recent years. Kabir et al. [23] developed a LSTM framework as a surrogate model of Euler-Bernoulli beam model and then used it in real-time SHM processes. In addition, Peringal et al. [24] used LSTM network to analyze the aircraft engine degradation patterns and schedule the maintenance.

Like RNN, LSTM is also a series of units that pass information and then model time series problems; the framework of one LSTM unit is shown in Figure 3. One commonly used approach is the vanilla LSTM sequence structure. Like RNN unit, a vanilla LSTM unit also includes an input X_t, hidden state H_t. In addition, it also includes a cell state C_t and has forget gate $f^{(t)}$, input gate $i^{(t)}$, and output gate $o^{(t)}$.

The input gate uses a sigma function to decide which parts of information should be kept and combined from current input X_t, output from previous Y_{t-1} and also the previous cell state C_{t-1}. On the opposite, the forget gate aims to use a sigma function to decide which information should be removed from current input X_t, output from previous Y_{t-1} and also the previous cell state C_{t-1}. Therefore, the formulas of input and forget gates can be written as follows:

$$i^{(t)} = \sigma(W_iX_t + U_iY_{t-1} + V_i \odot C_{t-1} + b_i) \tag{15}$$

and

$$f^{(t)} = \sigma\left(W_fX_t + U_fY_{t-1} + V_f \odot C_{t-1} + b_f\right) \tag{16}$$

In addition, the output gate formula is:

$$o^{(t)} = \sigma(W_oX_t + U_oY_{t-1} + V_o \odot C_{t-1} + b_o) \tag{17}$$

where $\odot$ are point-wise multiplication, W, U, and V are weight matrixes to get the update information and b is the constant bias. In input gate, these three weight matrixes help to filter information and pass to the next step, while they aim to remove information in forget gate. From input and forget gates, it is obvious that each LSTM unit can remove some useless information from previous unit, but just keep the useful information to update into next unit. Thus, it does

Figure 3
A vanilla LSTM unit

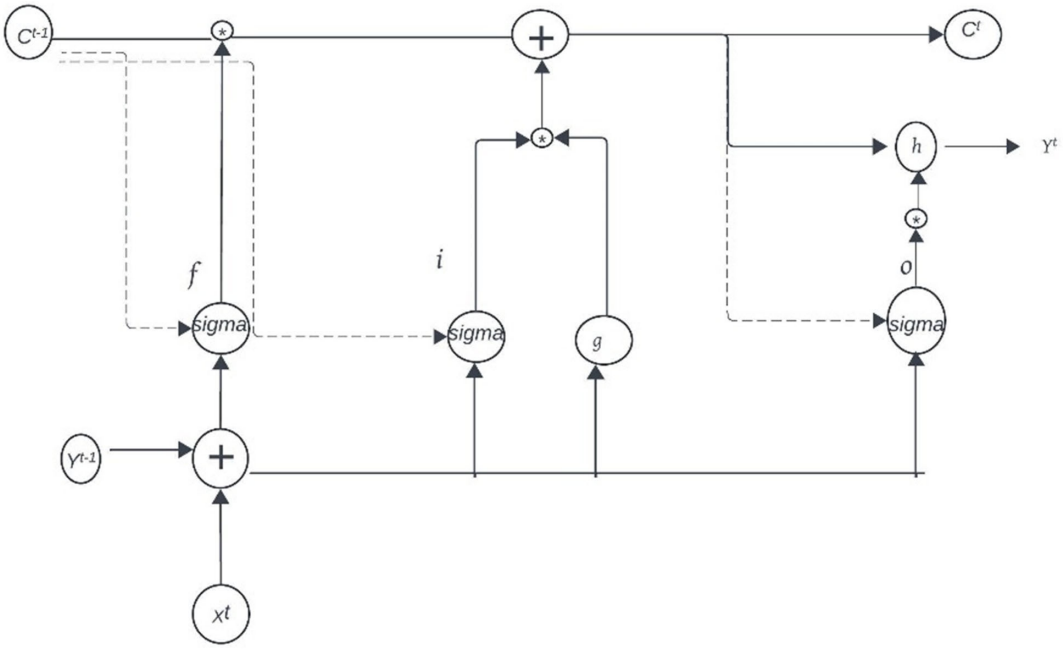

not need to keep all information from initial to final, and then it can avoid the gradient vanish issue in RNN chain structure.

The cell state allows information to be carried across many time steps without much change. This helps in preserving long-term dependencies and mitigating the vanishing gradient problem in standard RNN structure. The current cell state should be:

$$c^{(t)} = z^{(t)} \odot i^{(t)} + c^{(t-1)} \odot f^{(t)} \tag{18}$$

and $z^{(t)} = g(W_z X_t + U_z Y_{t-1} + b_z)$ is named block input.

Finally, the final estimation of LSTM will be the combination of current cell state with the output gate such that:

$$Y_t = g\left(c^{(t)}\right) \odot o^{(t)} \tag{19}$$

It finally predicts next time point target values Y_t based on all previous time points.

In this research, we will treat the cumulative strain $Cumu(\varepsilon_t)$ as current input variable X_t, and the RUL prediction should be Y_t. The values of weight matrixes and bias will be found by LSTM parameters optimization, and the detail will be discussed in Section 4.

4. Simulating Effect of Hurricanes on Building Behavior Using Wind Tunnel Testing

According to (ASCE 7–05) [25], residential building models scaled for wind tunnel testing typically range up to 1:50. Considering the dimensions of the wind tunnel test area, a two-story building with 7.5 meters height is scaled down to 0.16 m (~1:46 scale factor). This frame is constructed from pine wood with a Young's modulus of elasticity of 9 GPa.

To simulate the strong winds and hurricanes in the laboratory, a wind tunnel made by (Aerolab®) has been used. The strain measured by FBG sensors is collected by an FBG interrogator, which transmits the optical signals to a computer for visualization. Figure 4 provides a schematic diagram of the test setup, which includes the building

Figure 4
Schematic illustration of wind tunnel testing

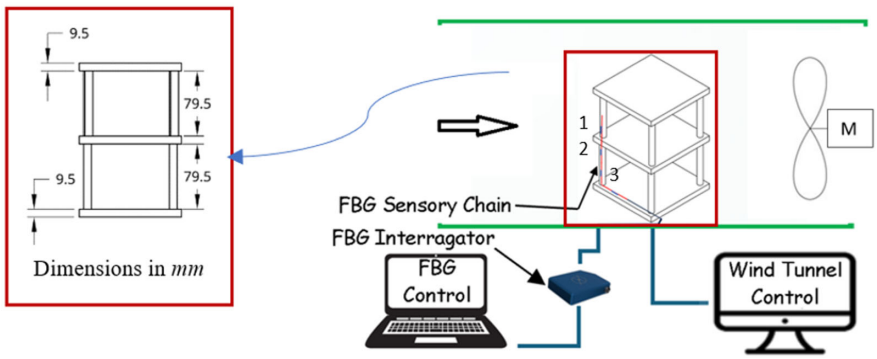

Figure 5
Strain measurement of the frames in wind tunnel

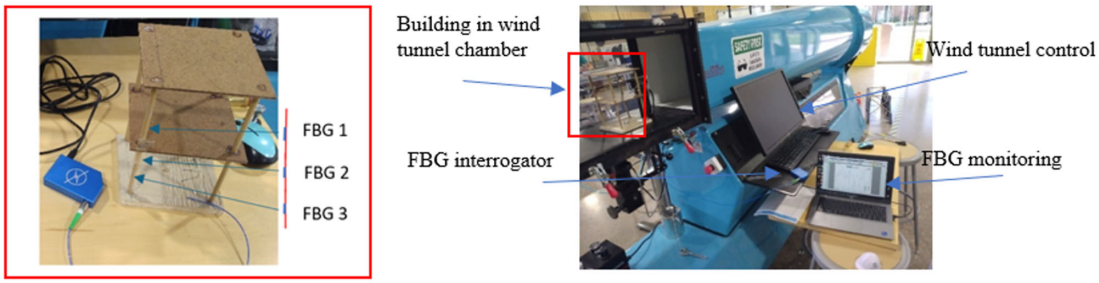

prototype, wind tunnel chamber, wind speed controller, FBG interrogator, and computer for visualizing the induced strain. Figure 5 shows the experimental setup showing the strain measurement using FBG sensors.

4.1. Discussions

In this section, the performance of the prototype building under various wind speeds and hurricane categories as given in Table 1 is investigated.

Table 1
Saffir-Simpson Hurricane categories

Designation	Wind speed, mph	Damage
Tropical depression	< 38	No damage
Tropical strom	39–73	Negligible damage
Hurricane		
Category 1	74–95	Some damage
Category 2	96–110	Extensive damage
Category 3	111–129	Devastating damage
Category 4	130–156	Catastrophic damage
Category 5	> 156	Catastrophic damage

4.2. Numerical strains

The induced strains at three different points along the column of the two-story building as shown in Figure 4 have been determined at various wind speeds and provided in Table 2 (Figure 4). As expected, the induced strains at all three points increase with higher wind speeds, due to the increased wind pressure as determined by Equation (6). The maximum strain occurs at the FBG sensor located 5 mm from the fixed support.

4.3. Experimental results

To demonstrate the performance and functionality of the building integrated with FBG sensors, the two-story structure with attached FBG sensors, as shown in Figure 5, was placed in a wind tunnel and subjected to various wind speeds. The wind speed was adjusted by controlling the fan's speed, ranging from 0 mph to 150 mph. It is worth noting that wind direction may affect the strain measured by FBG sensors. However, in the present study, the wind direction was kept constant due to limitations of the wind tunnel setup.

The numerical values of each FBG sensors are collected at desired sampling rate and saved in a.txt file. The files are exported and Figures 6 and 7 display the response of the FBG sensors at tropical depression and tropical storm respectively. As observed, FBGs 3 and 1 show the highest positive and negative values as they are connected close to the element's endpoints. It is observed that the strains at all points increase by increasing wind speed.

Figures 8 to 12 display the response of the FBG sensors at hurricane categories 1, 2, 3, 4, and 5, respectively. Once again, FBG 3 shows the highest value as it is located near the fixed support. It is observed that the strains at all points increase by increasing wind speed. It is observed that the strain values increase significantly from 22 μm/m to approximately 48 μm/m, more than doubling, when the hurricane category changes from 1 to 4.

5. LSTM Model Training and Prediction Results

As introduced in Section 2, a three-layer LSTM neural network model is trained in this study to estimate the unknown RUL of building structures and prevent potential damage. To optimize the prediction model, LSTM learning parameters are adjusted based on constant wind speed and varying wind speeds as outlined in

Table 2
Strain (μm/m) at the selected locations for two-story building

	Wind speed, mph						
FBG Location, mm	20	40	60	80 (Category 1)	100 (Category 2)	120 (Category 3)	140 (Category 4)
5	0.20	0.82	1.85	3.28	5.14	7.40	10.07
45	0.19	0.79	1.78	3.18	4.96	7.15	9.37
85	0.17	0.71	1.60	2.85	4.45	6.41	8.73

Figure 6
Strain measured by FBG sensors of a two-story frame at tropical depression (wind speed, < 37 mph)

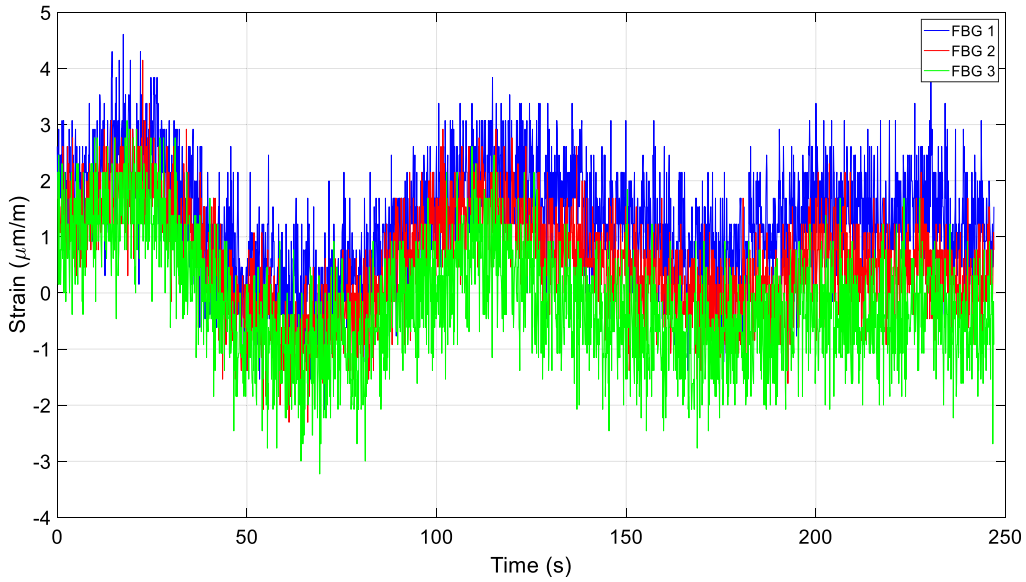

Figure 7
Strain measured by FBG sensors of a two-story frame at tropical storm (wind speed, 39–73 mph)

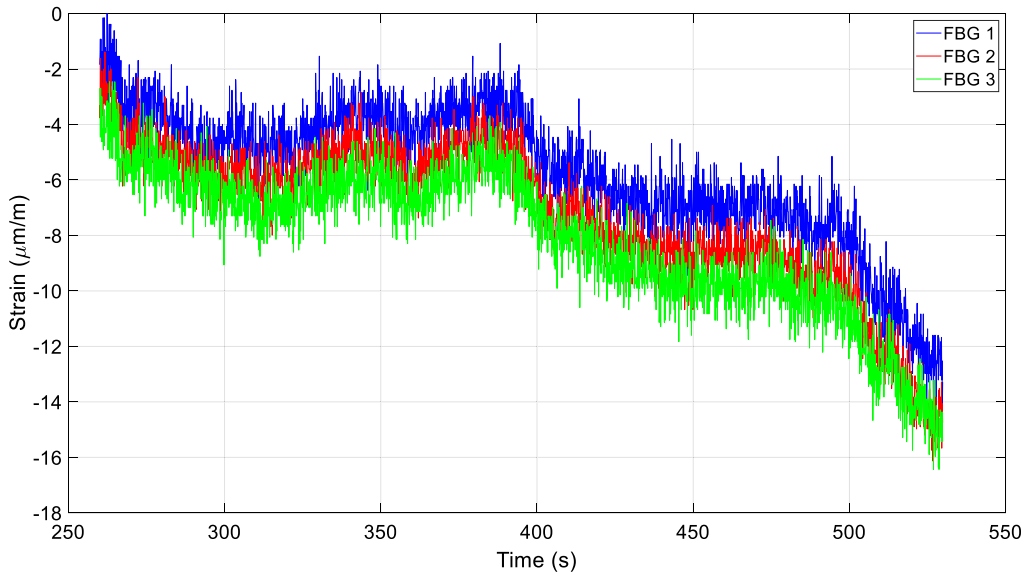

Figure 8
Strain measured by FBG sensors of a two-story frame at hurricane Category 1 (wind speed, 74–95 mph)

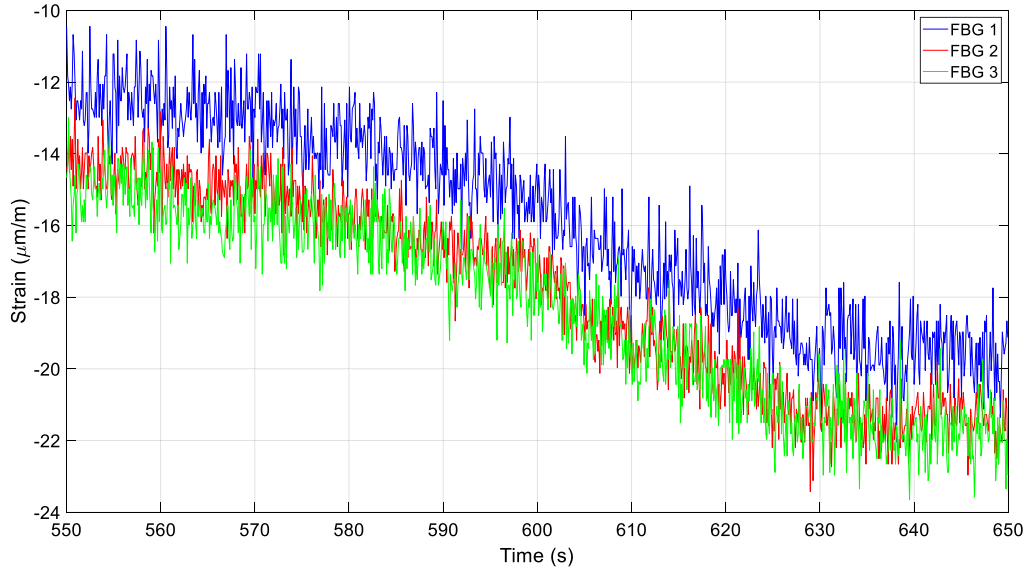

Figure 9
Strain measured by FBG sensors of a two-story frame at hurricane Category 2 (wind speed, 96–110 mph)

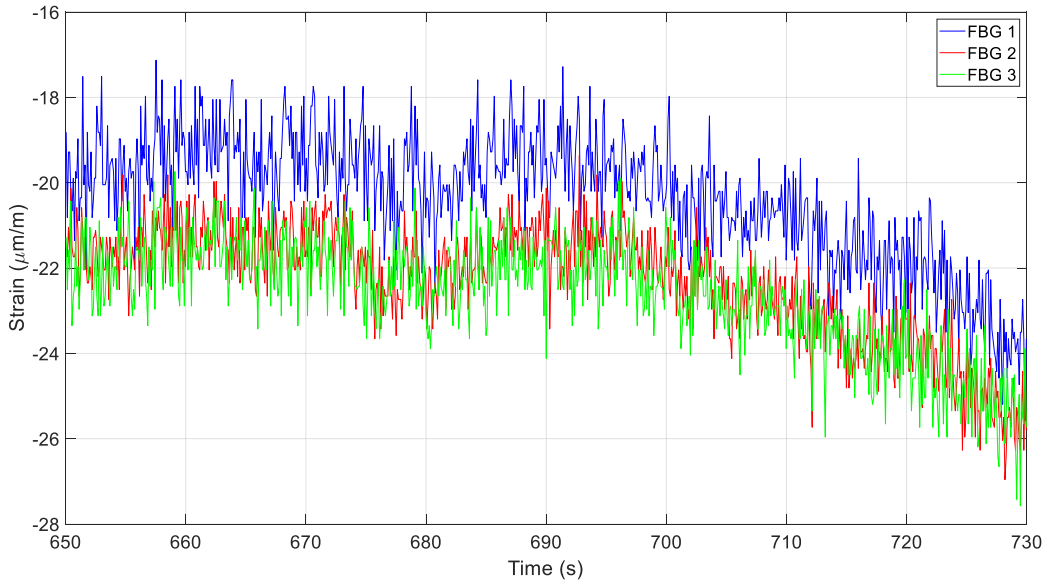

Figure 10
Strain measured by FBG sensors of a two-story frame at hurricane Category 3 (wind speed, 111–129 mph)

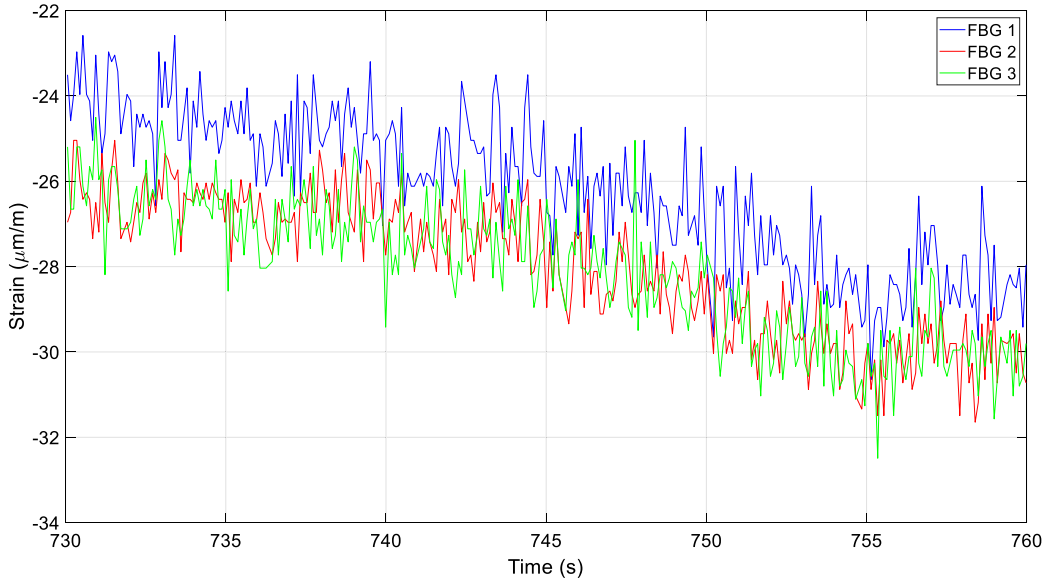

the designed experiments. Data preprocessing and model training were conducted using Python 3.11.5 on a Windows 11 platform with an Intel vPRO Essential i5 processor.

Under constant wind speed, the FBG sensors recorded 11,083 strain measurements over 1,114 s, with the maximum strain of 38.0978 occurring at the 9,838th record. According to Hooke's law, this represents the maximum strain the surface can withstand before failure occurs. Therefore, a new column is created to calculate the cumulative strain from the first record to the 9,838th record. The corresponding time at the 9,838th record is considered the failure time, and the RUL at this point is defined by Equation (8). Figure 13 illustrates the cumulative strain over time under constant wind speed conditions.

Typically, machine learning models require 70%–80% of the data for the training set and the remaining 20%–30% for the testing set. Since this study deals with a time series problem, we use data from the initial time $t = 0$ the 7,379th record as the training set, while the remaining 2,459 records are used as the

Figure 11
Strain measured by FBG sensors of a two-story frame at hurricane Category 4 (wind speed, 130–156 mph)

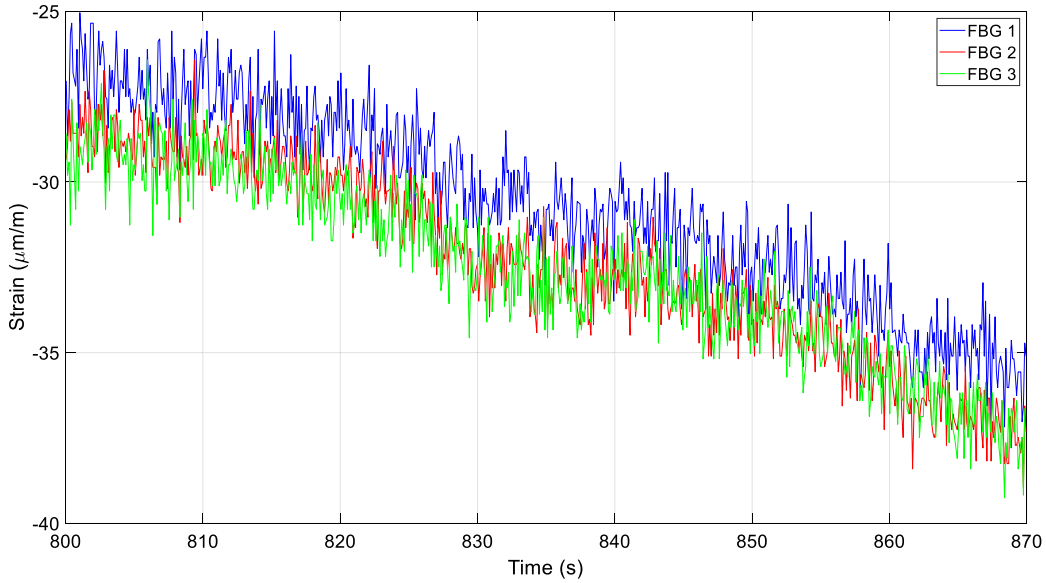

Figure 12
Strain measured by FBG sensors of a two-story frame at hurricane Category 5 (wind speed, >156 mph)

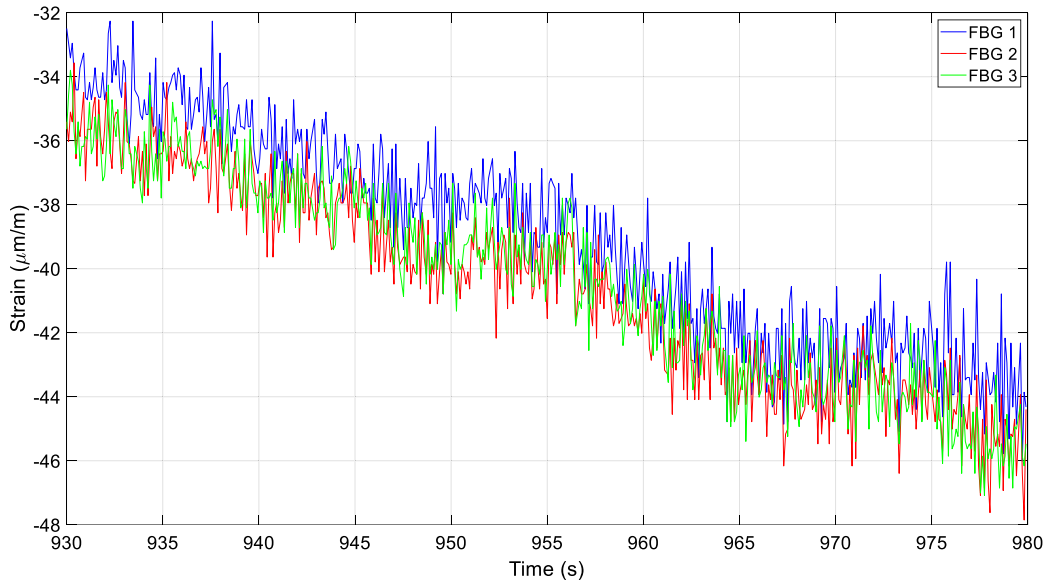

Figure 13
Cumulative strain under constant wind speed

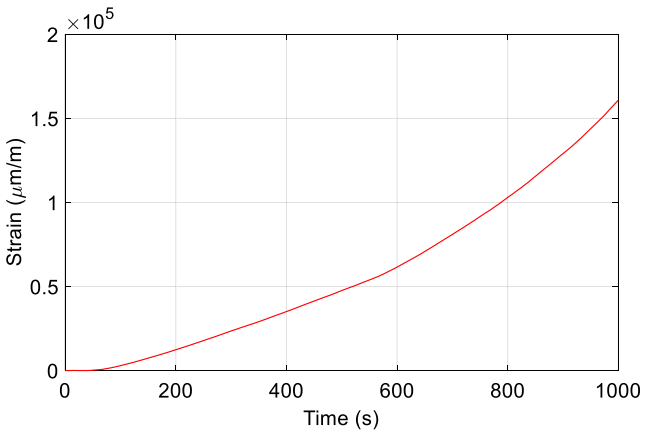

testing set. Additionally, 20% of the training data is further split as a validation set. In this LSTM model, we set LOOK_BACK = 1 since the prediction is based on the current point to forecast the next time point. The initial learning rate is set to 0.0001, and the optimal value is determined through grid search. The activation function used in the LSTM model is the hyperbolic tangent (tanh) function. Under constant wind speed conditions, the best-performing model is achieved with a 3-layer LSTM framework. The first LSTM layer contains 64 units, while the second and third layers each have 32 units. The activation function for all layers is the hyperbolic tangent (tanh) function. The performance results of the LSTM model under constant wind speed are displayed in Figures 14 and 15. Figure 15 shows the RUL model estimations are close to true value which means the model can perform prediction tasks well.

The model needs adjustments to accommodate dynamic wind speed conditions. Strain measurements were collected at wind

Figure 14
The training and validation loss of constant wind speed LSTM RUL prediction model

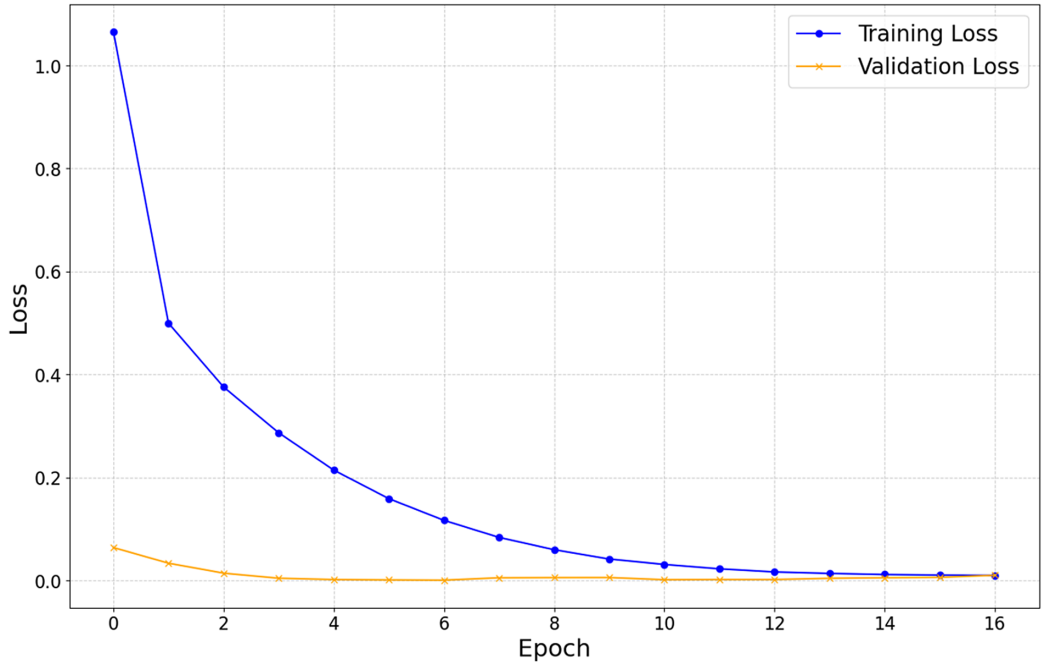

Figure 15
Remaining useful lifetime (RUL) prediction of constant wind speed via real testing values by LSTM neural network

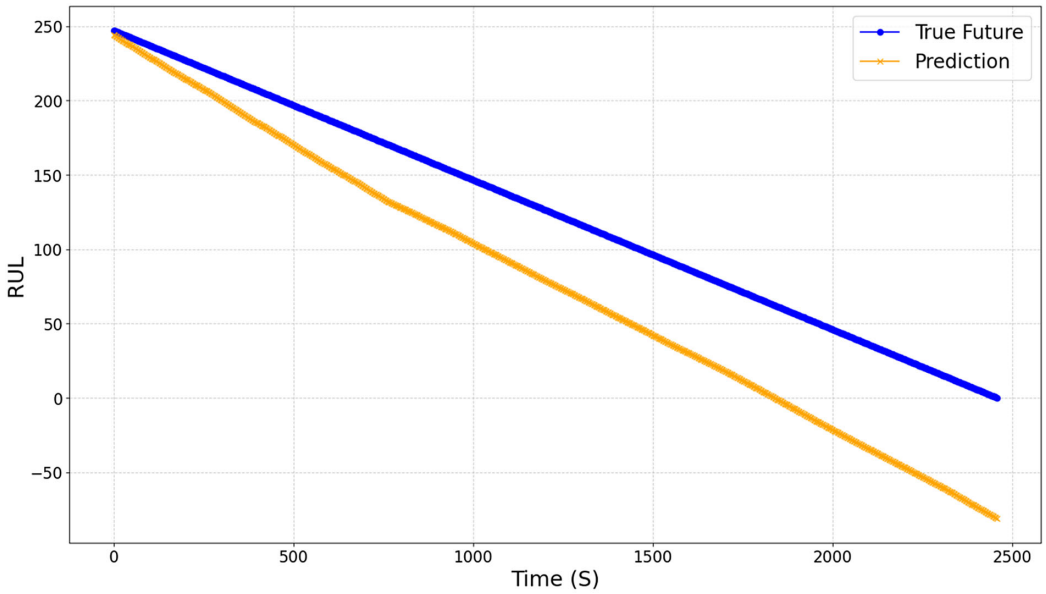

speeds of 0, 6.2, 31, 12.4, 108, 77.5, 93, and 151.9 RPM, so a variable for wind speed with 8 levels was introduced. Figure 16 shows the cumulative strain under dynamic wind speed. The deep learning model for RUL prediction now includes a numerical variable for cumulative strain and an ordinal variable for wind speed RPM. The LSTM framework and hyperparameters are then adjusted to optimize performance. We maintain a 3-layer LSTM structure, varying the number of units across 64, 128, and 256. The learning rate is selected from a range of 0.0001 to 0.001, with batch sizes of 32, 64, and 128, and epochs ranging from 50, 100, 120, to 150. Grid search is used to identify the best-performing model. The dynamic wind speed dataset consists of 5,246 rows of strain and wind speed measurements, with a maximum strain of 125.6613 occurring at the 3,018th record. According to Hooke's

Figure 16
Cumulative strain under dynamic wind speed

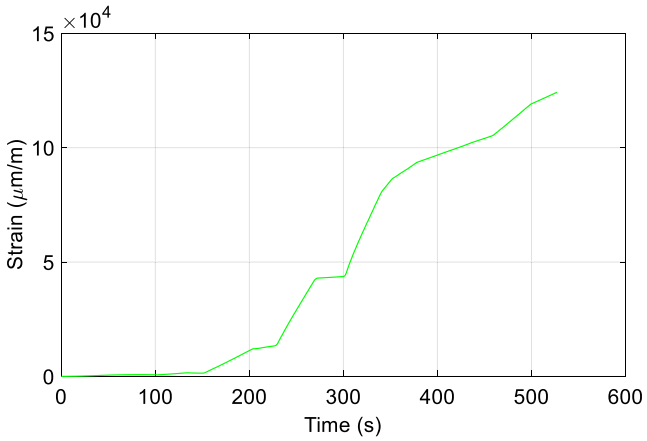

Figure 18
Remaining useful lifetime (RUL) prediction of dynamical wind speed via real testing values by LSTM neural network

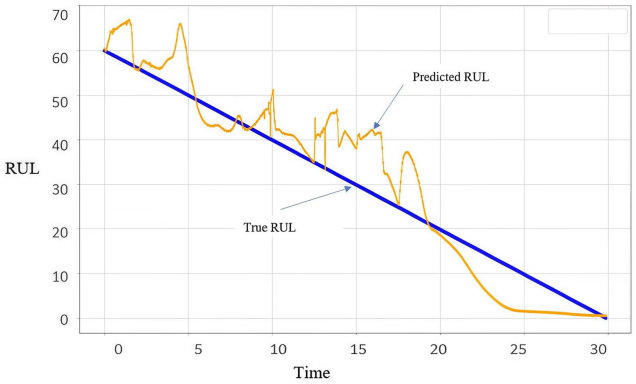

law, structural failure occurs at this point, with the RUL immediately dropping to zero.

Figure 17 shows the model loss result, it is obvious that training loss decreases steadily and approaches zero by around epoch 10. This indicates that the model is learning the training data very well. Even though there are some minor fluctuations in validation set as the epoch's progress, it still can show the stability of validation set.

Figure 18 shows the predicted RUL vs Time in second by LSTM model can have similar behavior as real RUL. The mean square error of the testing set is 483.5; and it can show the model provides enough information to help engineering people to keep maintenance of building structure on time.

6. Conclusion

The application of FBG sensors for monitoring the structural integrity of residential timber buildings has been explored. A two-dimensional frame element model was used to determine the induced strain in selected columns under varying wind speeds. A simplified wooden frame, designed to simulate timber structures, was placed in a wind tunnel and exposed to wind speeds ranging from 0 to 130 mph. The FBG sensors successfully captured strain data from key structural elements.

Furthermore, modal testing was performed to analyze the building's dynamic behavior, demonstrating that FBG sensors can

Figure 17
The training and validation loss of dynamical wind speed LSTM RUL prediction model

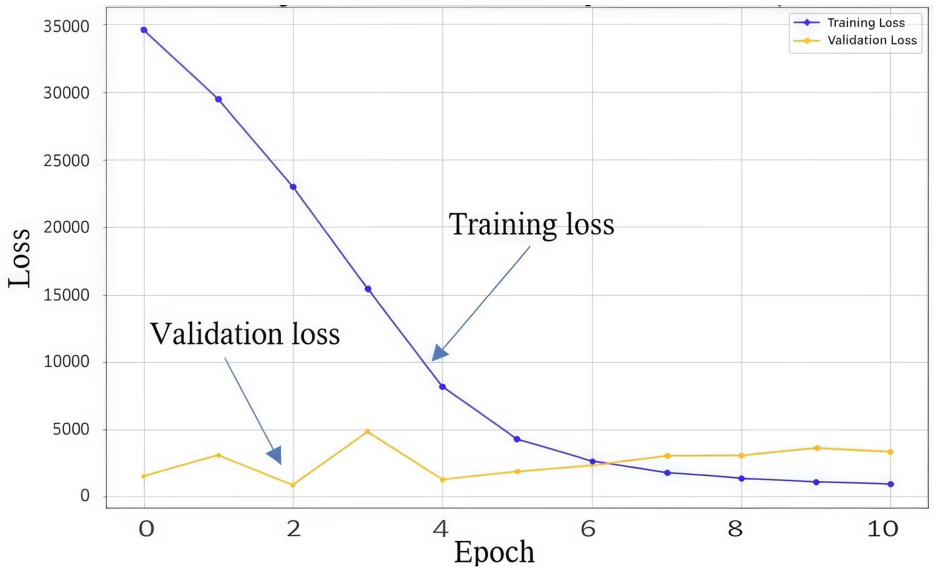

accurately measure real-time strain. The monitoring system was validated under both steady and fluctuating wind conditions. To estimate the RUL of the building, a three-layer LSTM neural network was employed. The strain data collected by the FBG sensors provided adequate input for model training. The LSTM model's predicted RUL is closely aligned with the actual RUL of the building, offering valuable information to help engineers perform timely structural maintenance.

Knowledge of a building's RUL can be utilized by local authorities to issue warnings, helping to prevent structural failures and safeguard lives during hurricanes. Additionally, insurance companies can leverage the RUL data to more accurately assess and determine structural insurance coverage.

Recommendations

The outcomes of this research revealed that SHM systems based on embedded FBG sensors provide low cost yet accurate monitoring systems for residential buildings. The mathematical model used to determine the level of reliability can be used to estimate the level of safety of the buildings subjected to strong winds and hurricanes. The present system can further be customized based on local weather and various types of buildings. It is recommended to use the present reliability system damage and safety model by local authorities and insurance companies.

Ethical Statement

This study does not contain any studies with human or animal subjects performed by any of the authors.

Conflicts of Interest

The authors declare that they have no conflicts of interest to this work.

Data Availability Statement

Data are available from the corresponding author upon reasonable request.

Author Contribution Statement

Abolghassem Zabihollah: Conceptualization, Validation, Investigation, Resources, Writing – original draft, Writing – review & editing, Visualization, Supervision, Project administration. **Yu Shi:** Methodology, Software, Formal analysis, Data curation, Writing – original draft, Writing – review & editing, Visualization.

References

[1] Park, G. (2021). A comprehensive analysis of hurricane damage across the U.S. Gulf and Atlantic coasts using geospatial big data. *ISPRS International Journal of Geo-Information*, *10*(11), 781. https://doi.org/10.3390/ijgi10110781

[2] Ayscue, J. K. (1996). *Hurricane damage to residential structures: Risk and mitigation* (Natural Hazards Research Working Paper No. 94). Natural Hazards Research and Applications Information Center. https://hazards.colorado.edu/research/working-papers/94

[3] Amirinia, G., & Jung, S. (2017). Buffeting response analysis of offshore wind turbines subjected to hurricanes. *Ocean Engineering*, *141*, 1–11. https://doi.org/10.1016/j.oceaneng.2017.06.005

[4] Abdulkarem, M., Samsudin, K., Rokhani, F. Z., & A Rasid, M. F. (2020). Wireless sensor network for structural health monitoring: A contemporary review of technologies, challenges, and future direction. *Structural Health Monitoring*, *19*(3), 693–735. https://doi.org/10.1177/1475921719854528

[5] Farrar, C. R., & Worden, K. (2007). An introduction to structural health monitoring. *Philosophical Transactions of the Royal Society A: Mathematical, Physical and Engineering Sciences*, *365*(1851), 303–315. https://doi.org/10.1098/rsta.2006.1928

[6] Sivasuriyan, A., Vijayan, D. S., Górski, W., Wodzyński, Ł., Vaverková, M. D., & Koda, E. (2021). Practical implementation of structural health monitoring in multi-story buildings. *Buildings*, *11*(6), 263. https://doi.org/10.3390/buildings11060263

[7] Maraveas, C., & Bartzanas, T. (2021). Sensors for structural health monitoring of agricultural structures. *Sensors*, *21*(1), 314. https://doi.org/10.3390/s21010314

[8] Park, G., & Inman, D. J. (2007). Structural health monitoring using piezoelectric impedance measurements. *Philosophical Transactions of the Royal Society A: Mathematical, Physical and Engineering Sciences*, *365*(1851), 373–392. https://doi.org/10.1098/rsta.2006.1934

[9] Ostachowicz, W., Soman, R., & Malinowski, P. (2019). Optimization of sensor placement for structural health monitoring: A review. *Structural Health Monitoring*, *18*(3), 963–988. https://doi.org/10.1177/1475921719825601

[10] Braunfelds, J., Senkans, U., Skels, P., Janeliukstis, R., Salgals, T., Redka, D., . . . , & Bobrovs, V. (2021). FBG-based sensing for structural health monitoring of road infrastructure. *Journal of Sensors*, *2021*(1), 8850368. https://doi.org/10.1155/2021/8850368

[11] Sliti, M., & Boudriga, N. (2021). Building structural health monitoring: An FBG-based estimation of external vibrations. In *2021 18th International Multi-Conference on Systems, Signals & Devices*, 1026–1031. https://doi.org/10.1109/SSD52085.2021.9429378

[12] Amaya, A., & Sierra-Pérez, J. (2022). Toward a structural health monitoring methodology for concrete structures under dynamic loads using embedded FBG sensors and strain mapping techniques. *Sensors*, *22*(12), 4569. https://doi.org/10.3390/s22124569

[13] Wu, T., Liu, G., Fu, S., & Xing, F. (2020). Recent progress of fiber-optic sensors for the structural health monitoring of civil infrastructure. *Sensors*, *20*(16), 4517. https://doi.org/10.3390/s20164517

[14] Zabihollah, A., Hajyalikhani, P., Ghorshi, S., & Vuddandam, R. (2024). Application of embedded FBG sensors for monitoring the structural stability of residential timber buildings under hurricane. In *Proceedings of the ASME 2024 Conference on Smart Materials, Adaptive Structures and Intelligent Systems*, V001T05A009. https://doi.org/10.1115/SMASIS2024-140408

[15] Liu, Z., Li, Y., Zhang, N., Liang, Z., & Li, F. (2021). Reliability analysis of CFRP-packaged FBG sensors using FMEA and FTA techniques. *Applied Sciences*, *11*(22), 10859. https://doi.org/10.3390/app112210859

[16] Hochreiter, S., & Schmidhuber, J. (1997). Long short-term memory. *Neural Computation*, *9*(8), 1735–1780. https://doi.org/10.1162/neco.1997.9.8.1735

[17] Elman, J. L. (1990). Finding structure in time. *Cognitive Science*, *14*(2), 179–211. https://doi.org/10.1207/s15516709cog1402_1

[18] Hou, G., Li, L., Xu, Z., Chen, Q., Liu, Y., & Qiu, B. (2021). A BIM-based visual warning management system for structural health monitoring integrated with LSTM network. *KSCE Journal of Civil Engineering*, *25*(8), 2779–2793. https://doi.org/10.1007/s12205-021-0565-0

[19] Zhang, H., Wang, L., & Shi, W. (2023). Seismic control of adaptive variable stiffness intelligent structures using fuzzy control strategy combined with LSTM. *Journal of Building Engineering*, *78*, 107549. https://doi.org/10.1016/j.jobe.2023.107549

[20] Miao, P., Yokota, H., & Zhang, Y. (2023). Deterioration prediction of existing concrete bridges using a LSTM recurrent neural network. *Structure and Infrastructure Engineering*, *19*(4), 475–489. https://doi.org/10.1080/15732479.2021.1951778

[21] Reddy, J. N. (2005). *An introduction to the finite element method* (3rd ed.). USA: McGraw-Hill Education.

[22] Sarkandi, G. I., & Zabihollah, A. (2011). A computational model for health monitoring of storage tanks using fiber Bragg grating optical fiber. *Journal of Civil Structural Health Monitoring*, *1*(3), 97–102. https://doi.org/10.1007/s13349-011-0010-z

[23] Kabir, E., Coble, D., Satme, J. N., Downey, A. R., Bakos, J. D., Andrews, D., & Huang, M. (2023). Accelerating LSTM-based high-rate dynamic system models. In *2023 33rd International Conference on Field-Programmable Logic and Applications*, 327–332. https://doi.org/10.1109/FPL60245.2023.00056

[24] Peringal, A., Mohiuddin, M. B., & Hassan, A. (2024). *Remaining useful life prediction for aircraft engines using LSTM*. arXiv. https://doi.org/10.48550/arXiv.2401.07590

[25] Mehta, K. C., & Coulbourne, W. L. (2010). *Wind loads: Guide to the wind load provisions of ASCE 7-05*. USA: American Society of Civil Engineers Press. https://doi.org/10.1061/9780784408582

How to Cite: Zabihollah, A., & Shi, Y. (2026). Reliability Analysis of Residential Buildings Under Hurricane Using Embedded FBG Sensors: Remaining Useful Lifetime Analysis. *Journal of Optics and Photonics Research*, *3*(2), 174–186. https://doi.org/10.47852/bonviewJOPR52024397